Finally, our data will help to fix the Pb yields from low-mass stars at low metallicities, that may then be used in models of the chemical evolution of the Galaxy (e.g., Travaglio et al. 1999). This would make the splitting between the s- and r-contribution to the solar Pb possible.

Acknowledgement

It is a pleasure to thank Dr. M. Kürster and the whole 3.6-m team for their operational support.

References

Aoki, W., Ryan, S.G., Norris, J.E., et al., 2001, *ApJ*, in press (astro-ph/0107040).

Biémont, E., Garnir, H. P., Palmeri, P., Li, Z. S. & Svanberg, S., 2000, *Mon. Not. R. Astron. Soc*. **312**, 116–122.

Burbidge, E.M., Burbidge, G.R., Fowler, W.A., Hoyle, F., 1957, *Rev. Mod. Phys.* **29**, 547.

Cayrel, R., Hill, V., Beers, T. C., et al., 2001, *Nature* **409**, 691.

Fujimoto, M.Y., Ikeda, Y., Iben, I.Jr. 2000, *ApJ* **529**, L25.

Gallino, R., Arlandini, C., Busso, M., et al., 1998, *ApJ* **497**, 388.

Goriely, S., Mowlavi, N., 2000a, *A&A* **362**, 599.

Goriely, S., Mowlavi, N., 2000b, in "The Galactic Halo: From Globular Clusters to Field Stars", A. Noels P. Magain, D. Caro, E. Jehin, G. Parmentier, A. Thoul (eds.), Proc. of the 35th Liège Intern. Astrophys. Coll. (Université de Liège, Belgium), 25.

Goriely, S., Siess, L., 2001, *A&A* **378,** L25.

Herwig, F., Blöcker, T., Schönberner, D., El Eid, M., 1997, *A&A* **324**, L81.

Kürster, M., 1998a, *The Messenger* **92**, 18.

Kürster, M., 1998b, *The Messenger* **94**, 12.

Langer, N., Heger, A., Wellstein, S., Herwig, F., 1999, *A&A* **346**, L37.

McClure, R.D., Woodsworth, A.W., 1990, *ApJ* **352**, 709.

Plez, B., Brett, J.M., Nordlund, A., 1992, *A&A* **256**, 551

Prantzos, N., Arnould, M., Arcoragi, J.-P., 1987, *ApJ* **315**, 209.

Travaglio, C., Galli, D., Gallino, R., et al., 1999, *ApJ* **521**, 691.

Van Eck, S., Jorissen, A., 1999, *A&A* **345**, 127.

Van Eck, S., Goriely, S., Jorissen, A., Plez, B., 2001, *Nature* **412**, 793.

SIMBA Explores the Southern Sky

L.-Å. NYMAN and M. LERNER, SEST and Onsala Space Observatory
M. NIELBOCK, M. ANCIAUX and K. BROOKS, ESO
R. CHINI, M. ALBRECHT and R. LEMKE, Astronomical Institute of Ruhr University of Bochum
E. KREYSA and R. ZYLKA, Max Planck Institute for Radio Astronomy
L.E.B. JOHANSSON, Onsala Space Observatory
L. BRONFMAN, Department of Astronomy, University of Chile
S. KONTINEN, Observatory, University of Helsinki
H. LINZ and B. STECKLUM, Thüringer Landessternwarte Tautenburg

SIMBA

SIMBA (the SEST Imaging Bolometer Array) was installed on the SEST in June this year through a collaboration between the University of Bochum, the Max-Planck-Institute for Radio Astronomy, the Swedish National Facility for Radio Astronomy and ESO. It is a 37-channel bolometer array operating at a wavelength of 1.2 mm.

Images produced by SIMBA are taken with the telescope in a fast scanning mode with speeds up to 160″/s without using a nutating subreflector. The beam size of SEST is 24″ at 1.2 mm and the pixel size in the SIMBA maps presented here is set to 8″. A map with a size of 15′ by 6′ with a rms noise of 40–50 mJy is obtained in only 12 minutes. More technical information about SIMBA is given on the SEST home page, and preliminary results were presented in ESO Press Release 20/01.

The strength of SIMBA is certainly the efficient coverage of large areas in a short time. It has therefore been used to map and survey regions of star formation in our own Galaxy as well as in nearby galaxies where cold dust and ionised regions emit strongly at 1.2 mm wavelength. SIMBA has also been used to study planetary nebulae, quasars, and maps of the deep fields in the Southern sky (the Hubble deep field South, the Chandra deep field, and the Phoenix deep field) have been obtained.

The SIMBA images presented in this article are preliminary in the sense that they were reduced with the on-line data reduction system. The data reduction software MOPSI – which so far has only been used for data obtained with a chopping secondary – is presently being adapted to the fast scanning mode and it is expected that all existing maps will improve in terms of intensity calibration and noise performance. Consequently, parts of extended, faint emission might have escaped detection so far but should appear more frequently after the upgrade.

The Orion region

Figure 1 displays the SIMBA map of the entire integral shaped Orion A molecular cloud complex at a wavelength of 1.2 mm. It has been created from 13 single maps during a total integration time of about 3.5 hours. The 1-sigma residual noise is about 40 mJy/beam.

The Orion A complex is usually divided into three regions, known as OMC-1, OMC-2 and OMC-3 (right panel), and the Orion Nebula (M 42) which belongs to the most luminous HII regions known. M42 is located in front of OMC-1 at a distance of 470 pc. This region also encompasses the brightest millimetre peaks of the SIMBA map, coincident with the Becklin-Neugebauer (BN) object adjacent to the Kleinmann-Low (KL) Nebula. The BN object is thought to be a young massive star of about 25 $L_{\odot}$ with a considerable mass loss.

Both M 42 and OMC-1 are regions of current massive star formation. OMC-1 itself is heated by stars from the nearby OB cluster within the Orion Nebula, including the Orion Trapezium. Its UV radiation is also responsible for photodissociation regions (PDR) on the surface of OMC-1 and southern parts of OMC-2.

OMC-2 and OMC-3 also show star-formation activity which is obvious from the numerous dense cores located within the filament. Some of them coincide with VLA radio sources, which is usually a sign of free-free emission from bow shocks of protostellar molecular outflows. In contrast to OMC-1, however, preferably low-mass stars are created there. Both OMC-2 and OMC-3 possess comparable amounts of gas and dust, although OMC-3 seems to be less evolved than OMC-2. Six of ten compact millimetre sources in OMC-3 have been identified as Class 0 protostars, while all sources in OMC-2 are at least of Class I. Furthermore, temperatures are lower and outflows are less

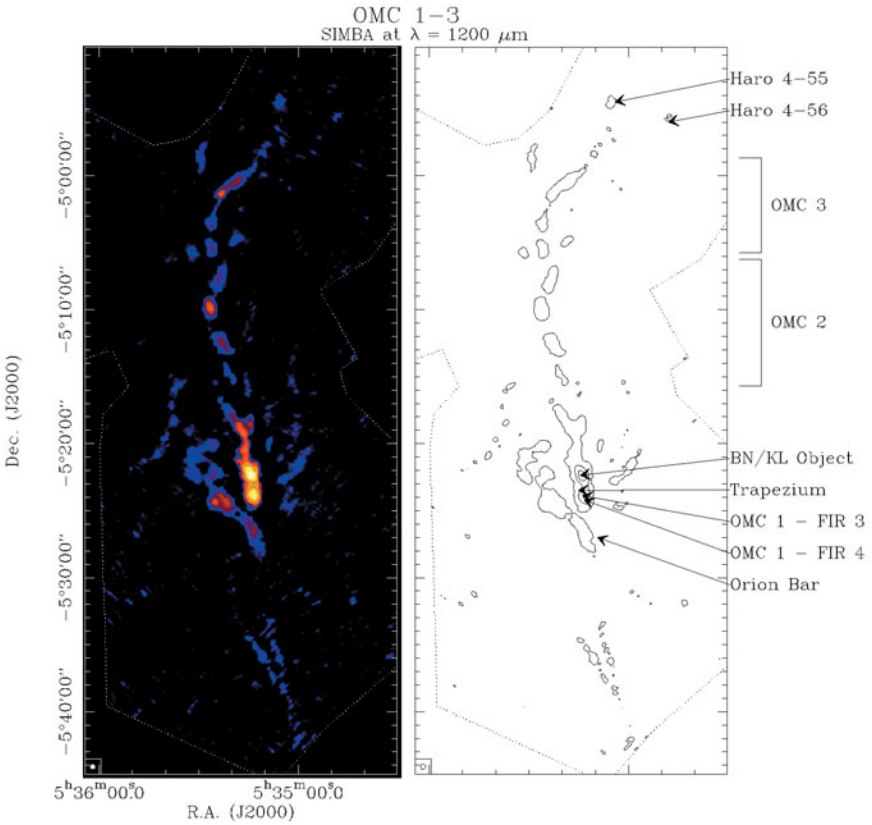

Figure 1: The Orion A molecular cloud complex. The left image shows the 1.2 mm SIMBA map. Some sources and regions of special interest are shown in the contour plot to the right. The circle in the lower or upper left corner seen in all figures except Fig. 4 depicts the SEST beamsize at 1.2 mm (24″ FWHM).

energetic in OMC-3 than in OMC-2. This suggests an evolutionary trend in the star formation history in Orion. Actually, it can be traced back to the Orion belt with a group of 6 to 12 Myr old stars. From there it advanced to the region of Orion's sword, where stars of 3 to 6 Myr age lie in front of the Orion nebula, where the next chapter of star formation took place. The evolution headed farther away from us to OMC-1, before turning back to the north and finally reaching the currently youngest region, OMC-3.

η Carinae and the Keyhole Nebula

The Keyhole Nebula is part of the Carina Nebula, an HII region/molecular cloud complex at a distance of 2.2 kpc. Herschel (1847) was the first to note the interesting optical features of the Keyhole Nebula which include bright arcs and filaments interwoven with dark patches, the most prominent of which is in the shape of a keyhole (see Malin 1993). The region is associated with Trumpler 16, an open cluster that contains numerous massive stars, including three O3-type stars as well as one of the most massive stars known – η Car. Such a high concentration of massive stars has created an extremely harsh environment within the Keyhole Nebula. There are bright ionisation fronts with complex kinematics and all that remains of the GMC in this region are externally heated molecular globules.

Figure 2 shows a SIMBA map of η Car and the surrounding regions. In addition to emission from η Car, there is a striking linear ridge of emission that extends more than 1 arcmin in length with a gap near the centre. Surrounding this ridge are a number of smaller emission clumps, one of which is located in the north and is in the shape of an arc that curves towards η Car. The emission detected by SIMBA closely follows the distribution of the 4.8-GHz continuum emission, which arises from thermal emission from ionised gas associated with one of the peaks in the Carina HII region (Car II). The main emission components are thought to be ionisation fronts possibly originating from η Car. It is not clear what is responsible for their striking shapes.

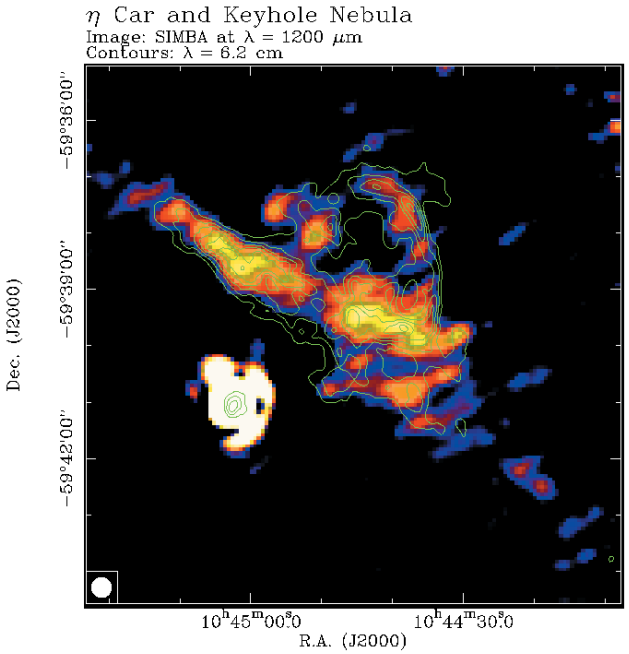

Figure 2: η Carinae and the Keyhole Nebula. η Carina is the bright region to the left in the map. The contours overlayed on the SIMBA map show the free-free emission from ionised gas at 4.8 GHz taken from a map obtained with the Australia Telescope Compact Array.

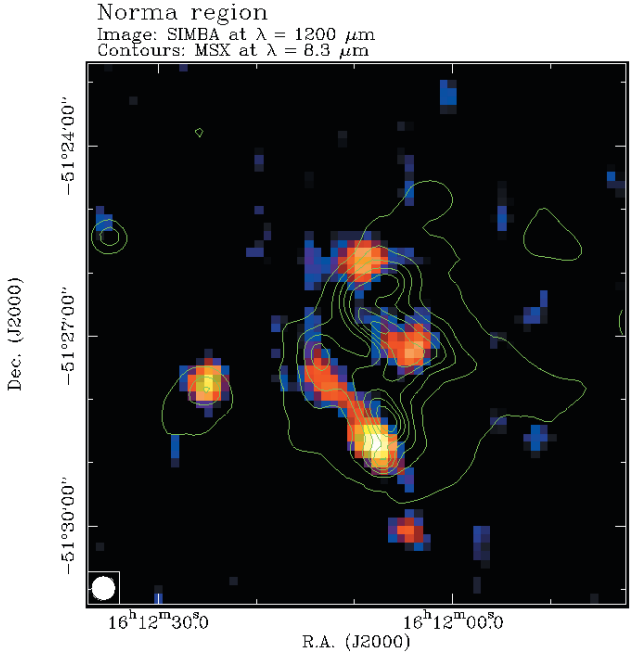

Figure 3: 1.2 mm emission from a dense core in the Norma spiral arm tangent point. The contours outline the 8.3 micron emission obtained with the MSX satellite.

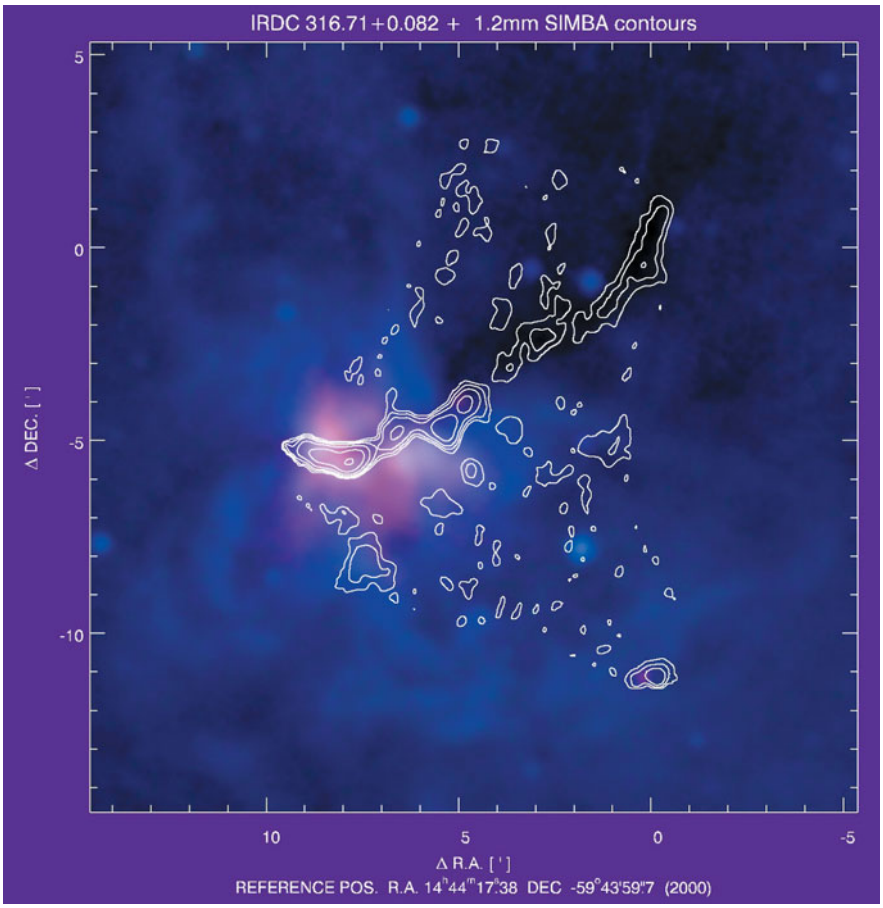

Figure 4: 1.2 mm emission from an infrared dark cloud. Contours from the SIMBA map are overlayed on a true colour MSX image.

Massive Star Formation in the Norma Spiral Arm

The Norma Spiral Arm contains the most massive molecular clouds as well as the most luminous regions of massive star formation in the Galactic disk. Eight embedded regions of OB star formation (identified in a survey of IRAS point sources with FIR colours of UC H II regions), situated in the spiral arm's tangent at $l \sim 330$ deg and at a distance of 7 kpc from the sun, have been previously mapped in CS(2-1) with the SEST. Figure 3 shows the SIMBA map of one of these dense cores; the most extended one (20 pc × 20 pc) observed so far in CS emission. As traced by SIMBA, it apparently contains UC HII regions, and more interestingly several massive stars in earlier stages of evolution. These data are consistent with a scenario of massive star formation occurring by fragmentation and condensation of the gas within the dense cores of giant molecular clouds.

Infrared Dark Clouds

The presence of a large number of so-called InfraRed Dark Clouds (IRDCs) was revealed by a mid-infrared survey of the Galactic plane conducted with the SPIRIT III instrument on board of the Midcourse Space Experiment (MSX). These clouds have MIR extinction values in excess of 2 magnitudes at 8 micron and are thought to contain cold ($T < 20$ K) and dense ($n(H_2) > 10^5$ cm^{-3}) material. Until now only a few IRDCs are examined in more detail. Several southern IRDCs were mapped with SIMBA to trace possible mm dust emission arising from the cold dust within the clouds. Figure 4 displays an interesting example of a non-spherical IRDC in the farther vicinity of a site of massive star formation. The contours are overlaid on a true colour MSX image which shows the 8, 13, and 21 micron emission coded blue, green, and red. The blue background results from the higher sensitivity and the ubiquitous PAH emission features covered by this band. This can be compared to the case of the Orion Trapezium region where the silhouette proplyds are seen against the optical emission. The superimposed SIMBA 1.2 mm contours in the right upper part match nicely the dark extincted region in the MSX image. A more extended lane of emission reaches down to the bright MIR region where several Galactic radio sources as well as OH, H_2O and methanol masers are located. Star formation probably started at the eastern end and spread along the filament. In fact, a very red source (which is not included even in the MSX catalogue) almost coincides with the 1.2 mm peak at the offset position (5′, –4′). It might be the youngest (massive) protostar seen so far.

The R CrA Star Forming Region

The Coronae Australis dark cloud complex is a nearby (130 pc) region of low-mass star formation. The cloud can be divided roughly into two parts; the north-western dense gas region, known as the R CrA core, and the south-eastern tail consisting of a quiescent dense core. The cloud complex is located 17 to 22 degrees below the galactic plane in a region which appears to be free of foreground or background dust and molecular gas.

A number of variable stars and embedded IR objects are associated with the R CrA Cloud. The brightest star, TY CrA (a Herbig Be star), has almost reached the main sequence. Others, like S CrA, T CrA, VV CrA and R CrA are still above the zero age main sequence. Some of the infrared objects have optical counterparts while some deeply embedded objects can only be detected in infrared. With SIMBA, it is possible to detect dust emission from small clumps giving rise to a single star or a stellar system and identify larger-scale dust structures.

The SIMBA data (shown in Fig. 5), taken together with the $C^{18}O$ and $C^{17}O$ column densities, can be used to estimate the degree of CO depletion onto dust grains. This is important because the freezing out of gaseous species onto grain surfaces strongly affects the physical and chemical properties of molecular clouds. This includes the deuterium fractionation and the degree of ionisation, one of the fundamental parameters regulating the rate of star formation, through the ion-neutral drift or ambipolar diffusion process. With SIMBA maps combined with spectral line observations, it is possible to correlate the dust emission characteristics with the degree of depletion and the chemical composition of dense clumps. This might reveal the importance of chemistry and depletion vs. desorption for the dynamical evolution of the cloud.

A region of 40′ times 20′ was observed with the SIMBA. The mapped area consists of 40 fast maps, varying from 400″ × 900″ to 792″ × 1400″ in size. The faint sources at the south-eastern quiescent core were resolved with 20 fast maps, which equals roughly 10 hours of observations. The other 20 scans were used to map the central and northwestern region of the cloud.

The Dark Globule B68

Stars form within dark clouds. While the study of protostars has been quite

successful during recent years, little is known about the initial conditions of star formation, i.e. the internal structure of the parental clouds. This is mainly due to the unknown amount of molecular hydrogen, which cannot be observed directly at the low temperatures of the clouds. The traditional way out of this dilemma was so far either to use tracer molecules such as CO and correlate their emission with the molecular hydrogen column density or to measure the optically thin emission of dust and derive the gas mass by adopting a gas-to-dust ratio. Both methods are based on a couple of assumptions on unknown conversion factors, which makes the determination of the amount of molecular hydrogen rather uncertain.

Recently, a new method to determine the line-of-sight distribution of dust in dark clouds has been applied successfully to some starless clouds like e.g. B 68 (Alves et al. 2001). The extinction could be directly measured from various IR colours towards background stars, yielding detailed maps of the dust column density. The penetrated optical depths (to a visual extinction of about 40 magnitudes) and the achieved spatial resolution (about 10) were an order of magnitude higher than previously possible from optical star count techniques.

Using these IR techniques in parallel to mm imaging seems to be an ideal tool to calibrate the mass absorption coefficient at 1.2 mm by comparing the IR-derived optical extinction with the mm-derived (optically thin) emission. Once this calibration has been established for a number of starless dust clouds, the total amount of dust can be determined for every dark cloud, independent of its optical depth and far beyond the capabilities of current IR techniques which are limited by the number of background stars detectable at high extinctions.

The application of this method is then wide spread. In particular, it allows to measure the total mass and the density structure of a cloud, the latter one on various scales from the global radial density profile until small-scale clumping. In addition, it is possible to study the initial conditions of star formation in a regime of optical depths where the current promising IR techniques cannot penetrate any longer the dust along the line of sight. Figure 6 shows a first example where we have mapped B 68 with SIMBA; the image consists of 130 coverages. From a preliminary analysis of the data and in comparison with the extinction map by Alves et al. (2001), we find that SIMBA traces the 1.2 mm emission until an equivalent optical extinction of 10 magnitudes; lower extinction values might be accessible soon when the reduction software has been optimised.

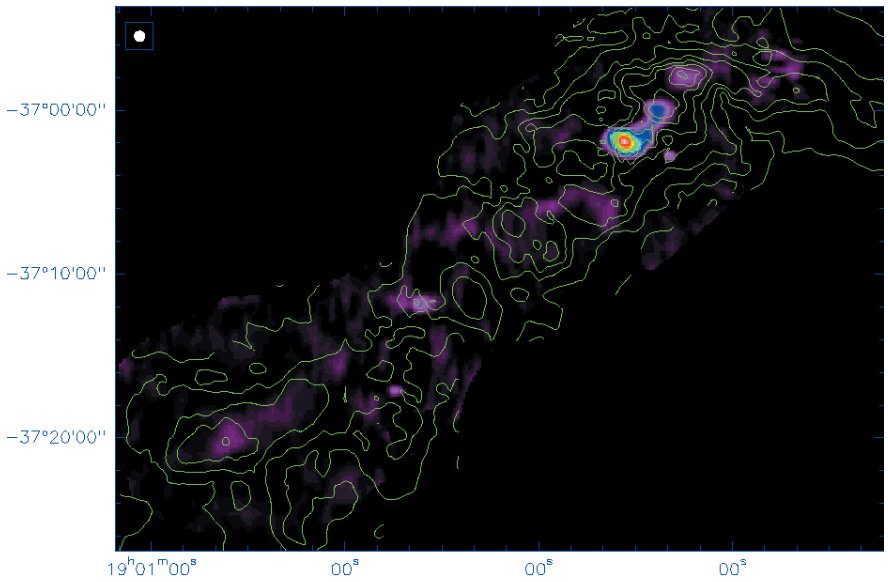

Figure 5: A SIMBA map of the low-mass star forming region R CrA. The contours show the integrated $C^{18}O$(1-0) emission from a map obtained by Harju et al. (1993) taken with the SEST. The lowest levels in the SIMBA map are set to reveal possible faint, extended structures.

30 Dor and N159 in the Large Magellanic Cloud

In Figures 7 and 8 SIMBA maps are presented of the 30 Doradus nebula (centred on the young cluster R 136) and an area including the HII region N 159 as well as prominent CO complexes. The distributions of the 1.2 mm flux are compared with those at 8.3 micron (from the MSX satellite) and the ^{12}CO(1-0) emission (obtained at SEST), respectively. Both regions show an excellent agreement between the 1.2 mm and 8.3 micron maps with respect to peak locations and extents, while the CO distribution, although closely associated with the 1.2 mm flux in general, deviates significantly in some cases. Most notable is the lack of 1.2 mm emission from the CO cloud south of N 159. CO excitation analysis indicates that this cloud is cold with kinetic temperatures probably less than 15 K. It is

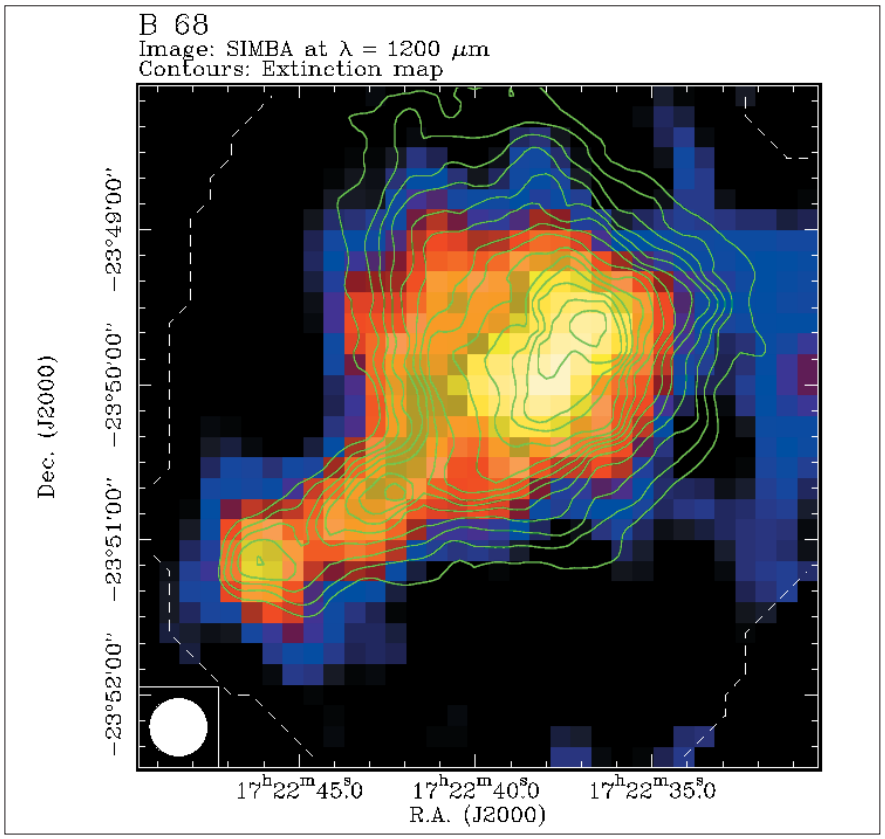

Figure 6: 1.2 mm emission from the dark globule B68. The contours are taken from the extinction map obtained by Alves et al. (2001).

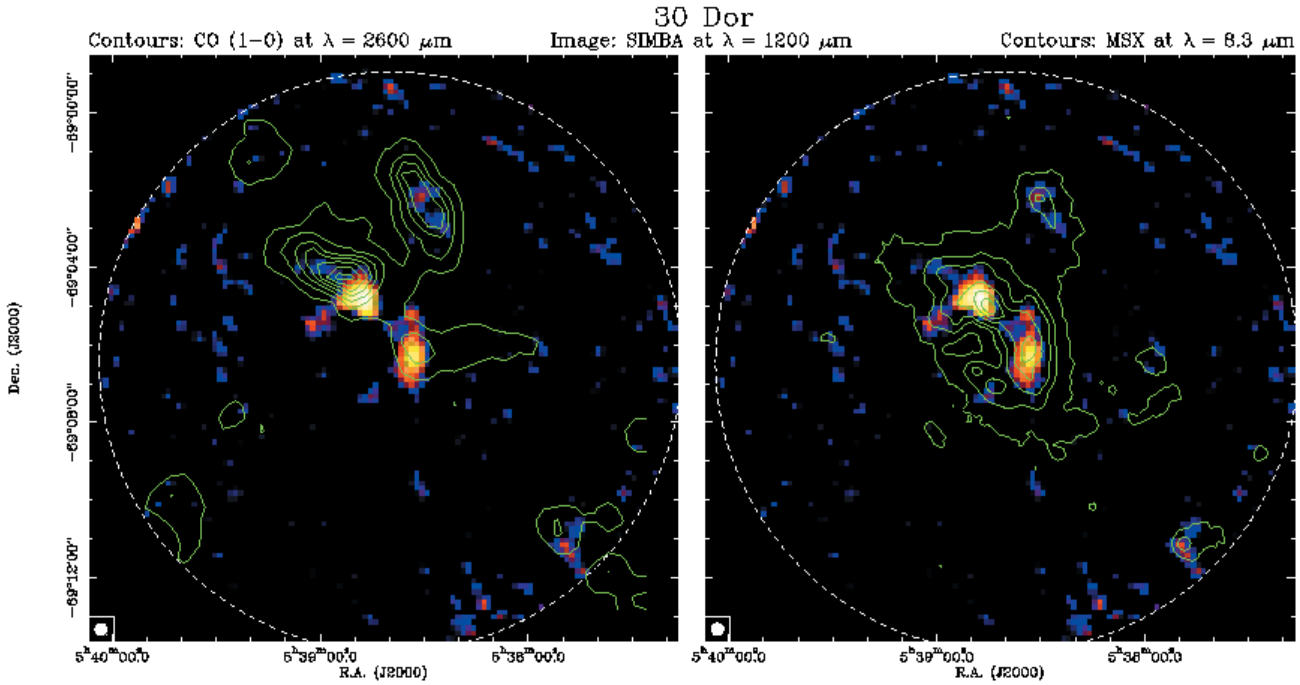

Figure 7: SIMBA 1.2 mm images of the 30 Dor region in the LMC. The contours show the integrated CO(1-0) emission (left panel), and the 8.3 micron contours from the MSX satellite image (right panel). The circle in the lower left corner depicts the SEST beamsize at 1.2 mm (24″ FWHM).

not associated with the formation of massive stars, in contrast to most of the CO complexes visible in these maps. The strongest 1.2 mm peak is associated with a region where the warmest CO cloud in the sample studied is located; according to the CO excitation analysis the kinetic temperature of this cloud is in the range 40–80 K.

Acknowledgements

We thank Joao Alves for permission to use the extinction map of B 68. We acknowledge the help of Katrin Kaempgen and Vera Hoffmeister for reducing the B 68 data. This article made use of data products from the Midcourse Space Experiment. Processing of the data was funded by the Ballistic Missile Defense Organization with additional support from NASA Office of Space Science. This article has also made use of the NASA/IPAC Infrared Science Archive, which is operated by the Jet Propulsion Laboratory, California Institute of Technology, under contract with the National Aeronautics and Space Administration.

References

Alves J., Lada C., Lada E., 2001, *The Messenger* No. 103.

Harju et al., 1993, *A&A* **278**, 569.

Herschel J.F.W., 1847, Results of Astronomical Observations at the Cape of Good Hope, London, p. 153.

Malin D., 1993, A View of the Universe. Cambridge University Press, pages 104, 155.

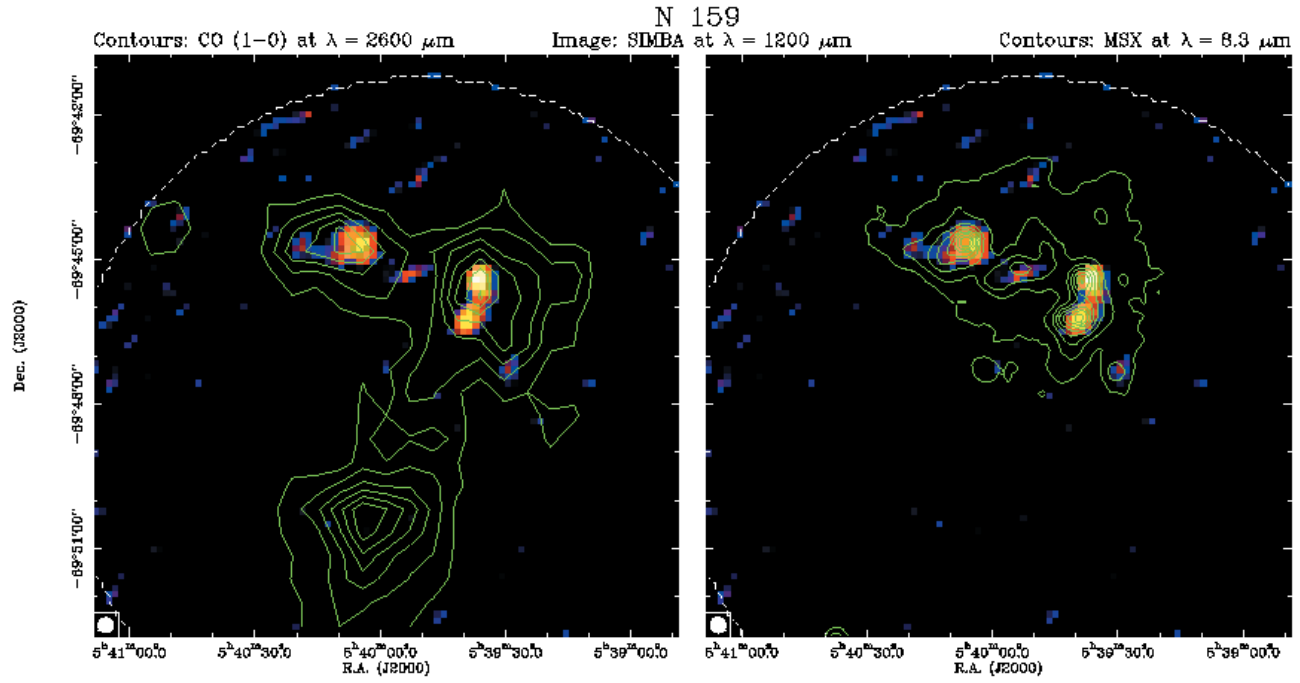

Figure 8: SIMBA 1.2 mm images of the N159 region in the LMC. The contours show the integrated CO(1-0) emission (left panel), and the 8.3 micron contours from the MSX satellite image (right panel).